iScience

CellPress
OPEN ACCESS

Article

Mechanotransduction in hippocampal neurons operates under localized low picoNewton forces

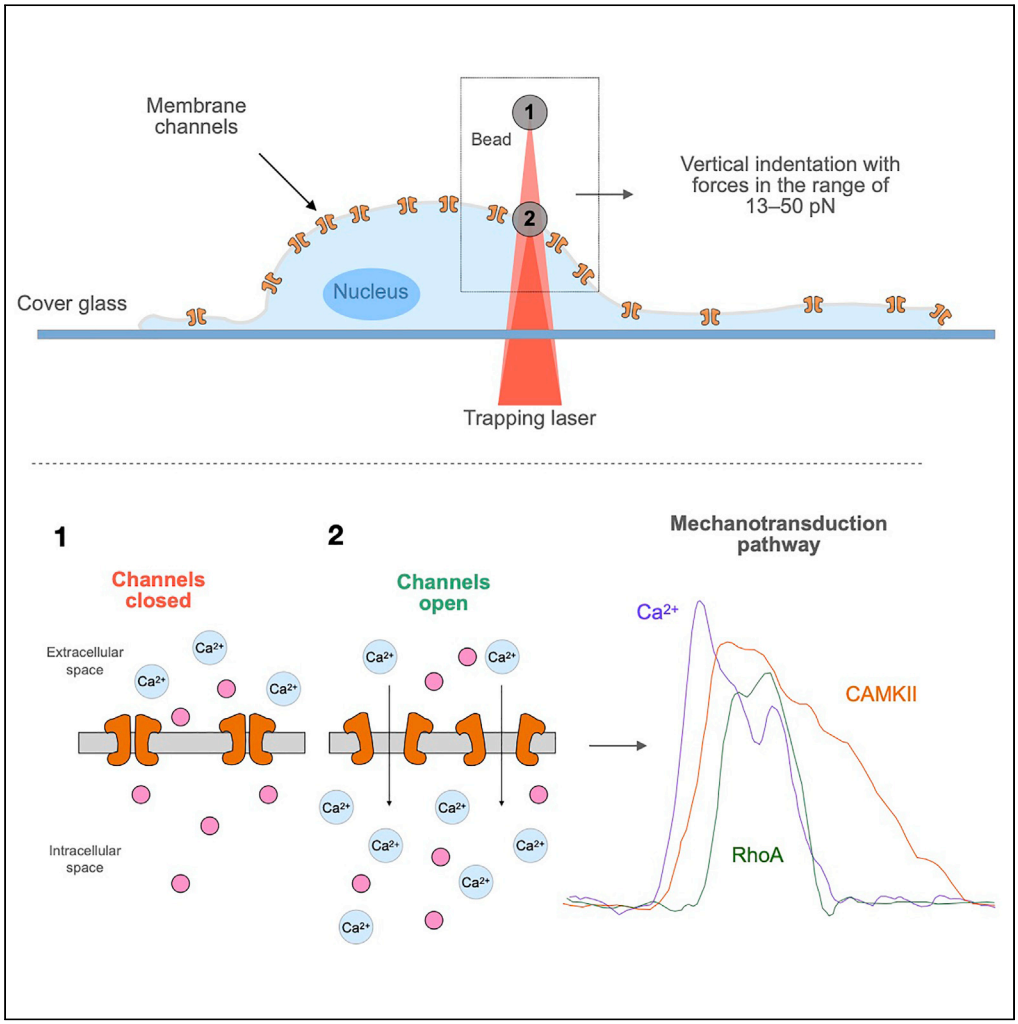

Fabio Falleroni, Ulisse Bocchero, Simone Mortal, Yunzhen Li, Zhongjie Ye, Dan Cojoc, Vincent Torre

fabio.falleroni@tum.de

Highlights

Hippocampal neurons are mechanically adapted to forces in the picoNewton range

Localized compressive mechanical stimuli in the range of 13–50 pN lead to Ca^{2+} influx

The evoked Ca^{2+} neuronal response is differentiated by the magnitude of the force

The subsequent mechanotransduction pathway involves the activation of CAMKII and RhoA

Falleroni et al., iScience 25, 103807
February 18, 2022
https://doi.org/10.1016/j.isci.2022.103807

iScience

CellPress
OPEN ACCESS

Article

Mechanotransduction in hippocampal neurons operates under localized low picoNewton forces

Fabio Falleroni,[1,3,5,*] Ulisse Bocchero,[2,3] Simone Mortal,[3] Yunzhen Li,[3] Zhongjie Ye,[3] Dan Cojoc,[4] and Vincent Torre[3,4]

SUMMARY

There is growing evidence suggesting that mechanical properties of CNS neurons may play an important regulatory role in cellular processes. Here, we employ an oscillatory optical tweezers (OOT) to exert a local indentation with forces in the range of 5–50 pN. We found that single local indentation above a threshold of 13 ± 1 pN evokes a transient intracellular calcium change, whereas repeated mechanical stimulations induce a more sustained and variable calcium response. Importantly, neurons were able to differentiate the magnitude of mechanical stimuli. Chemical perturbation and whole-cell patch clamp recordings suggest that mechanically evoked response requires the influx of extracellular calcium through transmembrane ion channels. Moreover, we observed a mechanically evoked activation of the CAMKII and small G protein RhoA. These results all together suggest that mechanical signaling among developed neurons fully operates in neuronal networks under physiological conditions.

INTRODUCTION

The neuronal mechanotransduction has been well studied at the level of several sensory neurons specialized to transduce mechanical stimuli that underlie hearing, mechanical sensation and pain (Marshall and Lumpkin, 2012; Lumpik and Caterina, 2007). The physical forces on sensory nerve ending open various ion channels such as mechanosensitive ion channels (MSCs) and the channel-like receptor TMC1/2 (Jia et al., 2020). Current investigations have shown that mechanosensitive channels (MSCs) are found almost ubiquitously in cells and tissues, suggesting that mechanosensitivity is widespread also in the central nervous system (CNS). Recently, mechanosensitivity has been shown to be established in hippocampal and cortical neurons (Nikolaev et al., 2015; Gaub et al., 2020) using different experimental methods. So far, in these experiments, the local applied force was quite high (above to 50 nN). In order to overcome this limit, here we employed an oscillatory optical tweezers (OOT) (Falleroni et al., 2018) able to exert a localized low picoNewton (pN) mechanical stimuli while monitoring the neuronal response. Specifically, we used the OOT to apply a local vertical indentation with forces in the range of 10–50 pN, which are dramatically smaller than the applied forces of the previous techniques. This is particularly important to study the neuronal mechanotransduction pathway at physiological force range considering that relevant molecular forces are typically in the picoNewton (pN) range. For instance, it has been demonstrated that cell adhesion molecules like cadherin and talin (Charras and Yap, 2018; Del Rio et al., 2009) or integrins receptors are sensitive to forces below 30 pN (Jurchenko et al., 2014; Kong et al., 2009). Microtubule and actin filaments typically generate pushing forces in the low pN range, when polymerizing against a barrier (Dogterom and Yurke, 1997; Footer et al., 2007). In addition, we have previously shown that filopodia and lamellipodia of neurons of the CNS exert small forces in the range of 2–50 pN (Cojoc et al., 2007; Amin et al., 2013). Therefore, it is important to establish the threshold of mechanosensitivity of central nervous neurons and, if this threshold is in the range of 10–50 pN, mechanical signaling could play a major role in the operation of neuronal networks.

In this study, we demonstrate that localized compressive mechanical stimuli at low picoNewton forces in the range of 13–50 pN applied to the hippocampal neuronal membrane can induce an intracellular calcium response. The amplitude of the evoked calcium transient scales both with the applied force and with the number of mechanical stimulations. Using chemical perturbation (BAPTA and GsMTx-4 treatment), we found that the mechanically evoked response of hippocampal neurons requires extracellular calcium entry from the extracellular space through transmembrane ion channels. In addition, we investigated the presence of inward

[1]Technische Universitat Munchen Fakultat fur Physik (TUM), 85748 Garching, Germany

[2]National Eye Institute (NEI), Bethesda, MD 20892, USA

[3]Neuroscience Area, International School for Advanced Studies (SISSA), 34136 Trieste, Italy

[4]Institute of Materials (IOM-CNR), Area Science Park, Basovizza, 34149 Trieste, Italy

[5]Lead contact

*Correspondence: fabio.falleroni@tum.de

https://doi.org/10.1016/j.isci.2022.103807

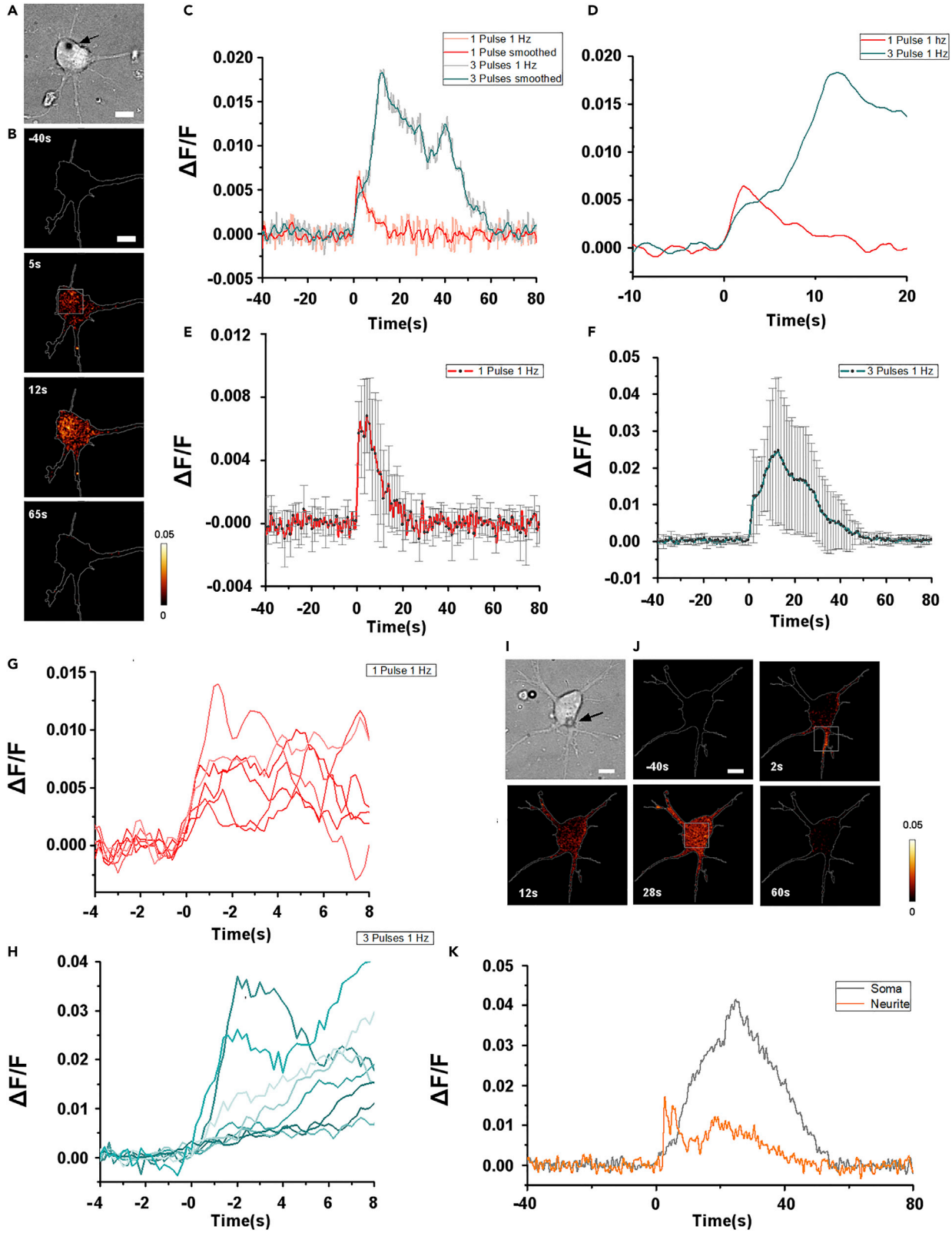
A
B
-40s
5s
12s
65s
0.05
0
C
1 Pulse 1 Hz
1 Pulse smoothed
3 Pulses 1 Hz
3 Pulses smoothed
ΔF/F
Time(s)
D
1 Pulse 1 hz
3 Pulse 1 Hz
ΔF/F
Time(s)
E
1 Pulse 1 Hz
ΔF/F
Time(s)
F
3 Pulses 1 Hz
ΔF/F
Time(s)
G
1 Pulse 1 Hz
ΔF/F
Time(s)
H
3 Pulses 1 Hz
ΔF/F
Time(s)
I
J
-40s
2s
12s
28s
60s
0.05
0
K
Soma
Neurite
ΔF/F
Time(s)

Figure 1. Calcium signals (DF/F) evoked by mechanical stimulation

(A) Bright-field image of hippocampal neurons with a trapped bead above the soma (black arrow).

(B) Time course of calcium transients evoked by three mechanical stimulations with one ROI used to compute the calcium signal (light gray box).

(C) Comparison of calcium transients evoked by one (red) and three (cyan) mechanical stimulations. The smoother lines represent running averages taken over a 2 s window.

(D) Enlargement of the smoothed traces in C for t = −10 s:20 s.

(E) Average and SD of calcium signals obtained with one mechanical pulse (n = 16).

(F) As in E but for three pulses (n = 10).

(G) Superimposed calcium signals obtained with one mechanical pulse.

(H) As in G but for three mechanical stimulations.

(I and J) As in A and B but for one experiment showing a calcium signal, both in the soma and neurite.

(K) Time course of calcium signals computed from the two ROIs (light gray box) shown in (J) Scale bar 5 μm. Data are represented as mean ± SD.

current using patch-clamp recording in whole-cell configuration and found a mechanosentitive current with maximum peak amplitude of 75 ± 17 pA. The presence of MSCs, such as Piezo1, in hippocampal neurons has been confirmed by immunochemistry. Whereas, we observed that the glia cells do not express Piezo1, but Piezo2. Interestingly, it has been demonstrated that Piezo1 is responsible for neurogenesis from neuronal stem cells because inhibition of channel activity by pharmacological or siRNA-mediated knockdown suppresses neurogenesis and enhances astrogenesis (Pathak et al., 2014). In addition, we observed mechanically evoked activation of CAMKII and the small G protein RhoA, reinforcing the idea that low mechanical stimuli are translated into biochemical signaling. This observation strengthens the idea that central neurons not only exchange electrical and chemical signals but also mechanical inputs. Additionally, we show that low picoNewton vertical mechanical stimuli act both on growth cones (GCs) inducing conformational changes. Our findings contribute to the fact that the central neuronal mechanotransduction pathway may be sensitive to physiologically compressive mechanical stimuli, characterized by low pN forces, as the one produced by a moving lamellipodium.

RESULTS

Mechanical stimuli trigger an elevation of intracellular calcium

To test whether hippocampal neurons respond to low picoNewton mechanical stimulation (10–50 pN), we used the intracellular calcium dye Fluo-4-AM. To mechanically stimulate the neuron, a 3.5 μm polystyrene bead was trapped and positioned above the soma close to the initial segment of the largest neurite (Figure 1A). Images of the emitted fluorescence (F) were acquired for about 3 min and, if F was stable, we proceeded with the mechanical stimulation. The trapped bead was lowered vertically to touch the cell membrane and then retracted with a 200 nm step. A fixed number of oscillations (from 1 to 3, 1Hz) with an amplitude of 1 μm was then applied to the optical trap. In this way, we applied controlled mechanical stimulations during which both the force and the indentation were independently measured by the quadrant position detector (QPD).

Initially, we mechanically stimulated the hippocampal neurons using a single local indentation with a stiffness K of 0.14 pN/nm corresponding to a maximum force of 50 ± 2 pN and an indentation of 360 ± 12 nm on the plasma membrane. We observed a rapid and transient intracellular calcium signal. The evoked calcium signal occurred within 300 ± 100 ms and returned to baseline fluorescence levels after 20 s on average (red trace in Figures 1C, 1D, and 1E). In these experiments, the evoked calcium signal showed a peak fluorescence increase (DF/F) of 0.0068 ± 0.002 (Figure 1E, n = 16). In total, 45% of the neurons responded to single mechanical indentation. We next applied a mechanical stimulation composed of three pulses with the same stiffness previously used (K: 0.14 pN/nm, 50 ± 2 pN). We observed an increase in $[Ca^{2+}]_i$ in a highly localized manner near the site of the mechanical stimulation. Then, within some seconds, the initial component was followed by a second larger evoked calcium change (DF/F peak: 0.028 ± 0.008, n = 14) with a mean duration of approximately 60 s (Figures 1C and 1F). Here, the 65% of the neurons responded to repetitive mechanical indentation.

We aligned the time course of the evoked changes in $[Ca^{2+}]_i$ from different neurons (different colors in Figure 1G for one pulse (n = 6) and in Figure 1H for three pulses (n = 8) to the onset of mechanical stimulation. A closer inspection of these responses shows several important features of mechanotransduction. Specifically, we observed that the onset of the initial component occurred within 300 ± 100 ms, following mechanical stimulation regardless of whether one or three pulses were used. Moreover, the amplitude of the initial component was remarkably similar in different neurons with a DF/F of

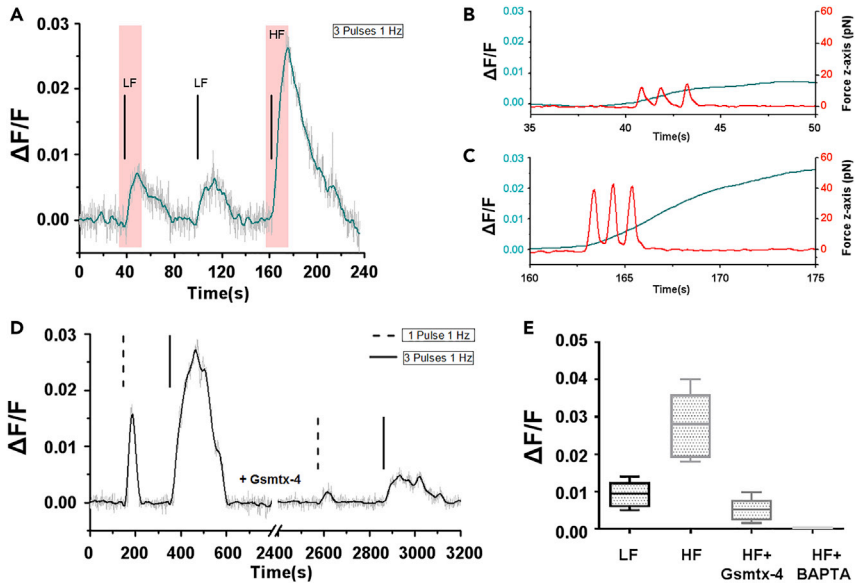

Figure 2. Calcium signals evoked by mechanical stimulations with different magnitude

(A) Time course of the evoked calcium signals by mechanical stimulation with a low force (LF) equivalent to 13 ± 1 pN and a high force (HF) equivalent to 50 ± 2 pN.

(B and C) Enlargement of the traces in A (red light boxes) showing the time course of the mechanical stimulations and of the induced calcium signals.

(D) Effect of GsMTx-4 (10 μM) on mechanically induced calcium signals. The broken line in the x axis indicates the time of drug application (2400 s).

(E) Statistics of calcium transient DF/F for three pulses with a trap stiffness of k = 0.046 pN/nm (LF) and k = 0.14 pN/nm (HF), HF + GsMTx-4 (10μM), and HF + BAPTA (2 mM) treatment. Data in (E) are represented as mean ± SD.

approximately 0.01, while the slow and delayed component developed with a variable delay from one up to 5 s. In conclusion, the amplitude of the delayed component was highly variable, in contrast with the amplitude and delay of the initial component, which were reproducible (Figures 1G and 1H). The comparison of the DF/F averaged over different neurons for one (Figure 1E) and three pulses (Figure 1F) shows that the response to three mechanical pulses is often larger than 3 times the response to one pulse and it has a more complex shape (0.0068 ± 0.002 DF/F vs 0.028 ± 0.008 DF/F). Moreover, we observed that repetitive mechanical stimulation induced a calcium response in the neurite close to the site of stimulation in 30% of the stimulated neurons (Figure 1K). Notably, the mechanically evoked calcium showed a different time course in the neurite and the soma (compare orange and light gray trace in Figure 1K). Differently from the soma, the mechanical stimulation evoked in the neurite a transient response which returned to baseline levels within about 10 s with a peak fluorescence increase (DF/F) of 0.012 ± 0.005 (n = 4). The occurrence of the calcium response was not observed when the bead oscillated in close proximity of the neuron without touching it, as revealed by the QPD signal. Therefore, the intracellular calcium change is a genuine biological event and does not originate from optical interference caused by bead motion.

Next, to determine the lowest mechanical force able to activate a detectable response, we applied both one and three mechanical pulses using a trap stiffness of 0.046 pN/nm equivalent to a force of 13 ± 1 pN referred to as LF (low force) and an indentation of 280 ± 18 nm on the plasma membrane. In this case, the single mechanical stimulation did not induce any significant detectable Ca^{2+} signal whereas three pulses evoked calcium response with a peak fluorescence increase (DF/F) of 0.009 ± 0.003 (n = 8). In total, 40% of the neurons responded to repetitive mechanical indentation with the low-force regime. This calcium response is more than 3 times minor than the one obtained with higher forces (K: 0.14 pN/nm, 50 ± 2 pN) (Figures 2A, 2B, 2C, and 2E).

Taken together, these results indicate that the threshold for evoking a detectable change in $[Ca^{2+}]_i$ is approximately 13 pN and that neurons can differentiate the amplitude of applied force.

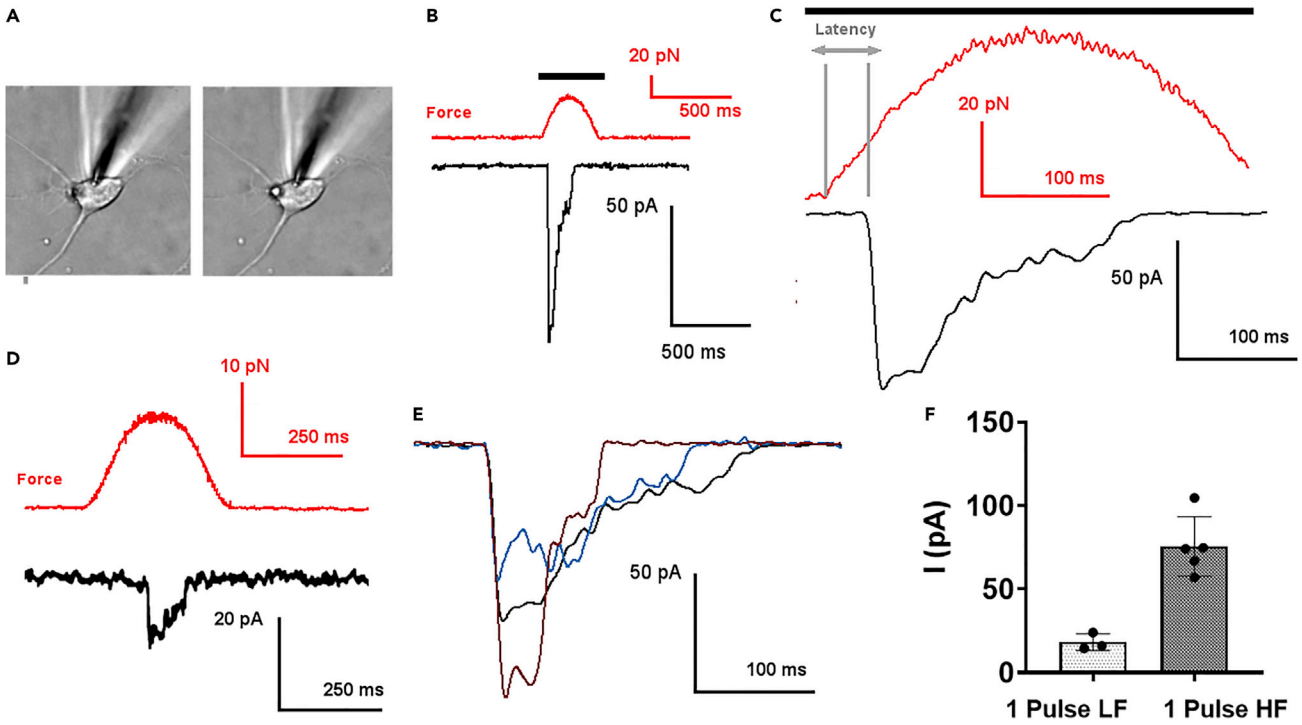

Figure 3. Mechanosensitive inward current in hippocampal neuron

(A) Bright-field images of voltage-clamped hippocampal neuron in whole-cell mode (electrode) and mechanically stimulated by a polystyrene bead.

(B) Indentation of cell membrane with high-force regime (HF) results in rapidly activating inward current (black trace); red trace indicates the force applied through the bead to the cell membrane.

(C) Enlargement of traces in B showing how mechanical latency and force threshold were measured.

(D) As in B but for mechanical stimulation with low-force regime (LF).

(E) Superimposed inward mechanosensitive current aligned for the onset obtained with one mechanical pulse with high-force regime.

(F) Statistics of inward currents evoked by for one pulse with a trap stiffness of k = 0.046 pN/nm (LF) and k = 0.14 pN/nm (HF). Data in (F) are represented as mean ± SD.

Next, to gain more insight, we decided to verify whether blockage of mechanosensitive channels (MSCs) eliminated or reduced the amplitude of the evoked Ca^{2+} transients. Therefore, we used the MSC inhibitor GsMTx-4. GsMTx-4 is a small peptide obtained from spider venom and has been shown to inhibit MSCs from both the Piezo and TRP families (Gnanasambandam et al., 2017). This inhibitor acts at the interface between the lipids in which the MSC is embedded, thereby reducing the effective magnitude of the mechanical stimulus acting on the MSC gate; thus, GsMTx-4 is a gate modifier rather than an ion pore blocker. In six experiments, following the observation of calcium transients evoked by mechanical stimuli, 10 μM GsMTx-4 was added to the medium and the mechanical stimulation was repeated (Figure 2E). In the presence of GSMTx-4, the amplitude of calcium transients was significantly reduced in 40% of the mechanically stimulated neurons (0.02 ± 0.008 vs 0.005 ± 0.0015 for the three pulses stimulation, n = 6) (Figure 2D). These results suggest that the calcium response mechanically evoked in hippocampal neurons are partially mediated by canonical MSCs in the plasma membrane.

Next, in order to investigate the mechanism of mechanically evoked calcium response, we used the cell-impermeant calcium chelator BAPTA. Application of BAPTA completely abolished the neuronal calcium response to localized mechanical stimulation composed by three pulses with high-force regime (DF/F of 0.0 ± 0.0, Figure 2E, n = 6). These results suggest that calcium influx across the membrane is essential for the mechanically evoked response.

Then, to gain insight into the mechanism underlying the calcium response, we performed whole-cell patch clamp recording searching for mechanically activated mechanosensitive currents. In these experiments, we placed the probe for patch-clamp recordings at about 5 μm from the stimulation site (Figure 3A).

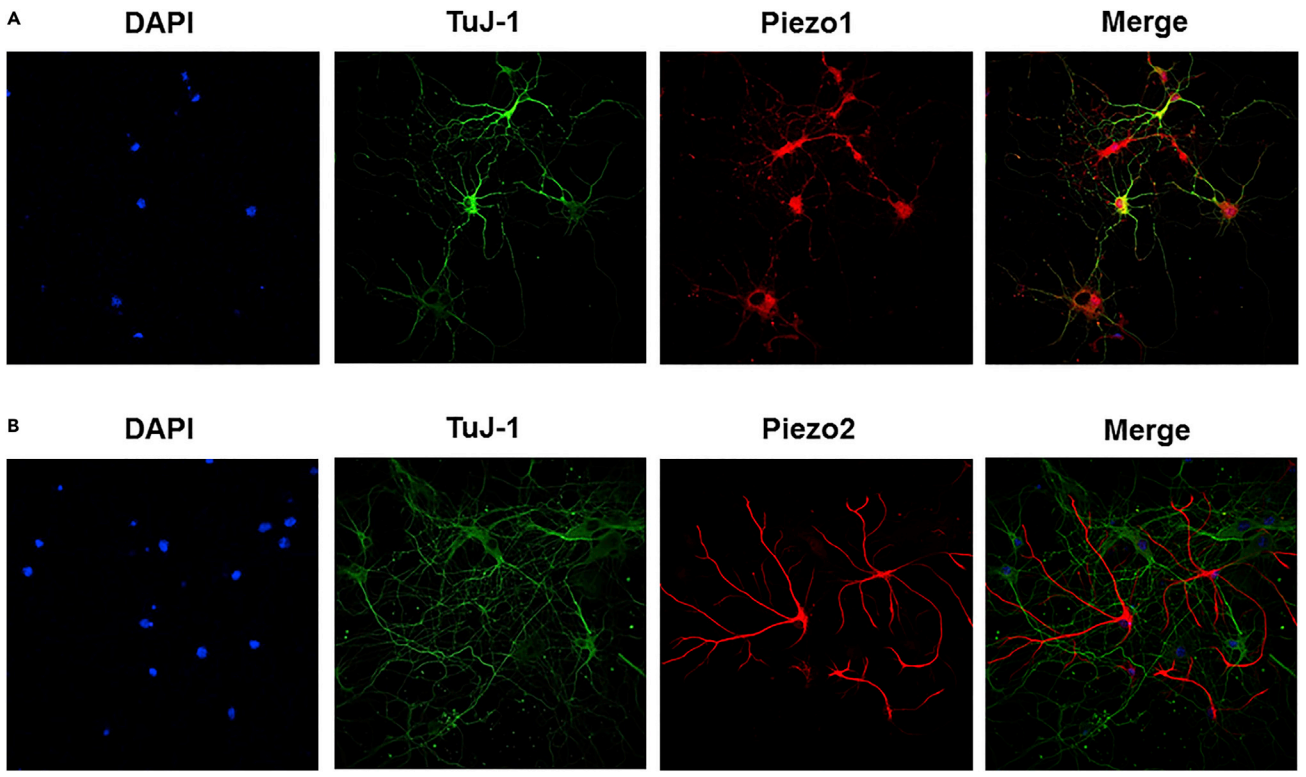

Figure 4. Expression of mechanosensitive channels in hippocampal neuronal cultures

(A) Immunofluorescence images showing the neuronal markers TuJ-1, Piezo1, DAPI, and the merged signals. The staining of Piezo1 colocalizes with TuJ-1.
(B) As in (A) but for Piezo2. Piezo2 is mainly expressed in glial cells.

Then, we first mechanically stimulated the hippocampal neurons using a single local indentation with a stiffness K of 0.14 pN/nm corresponding to a maximum force of 50 $\pm$ 2 pN (Figures 3B and 3D). In 35% of the stimulated hippocampal neurons, we found an inward current mechanically evoked with an average amplitude of 75 $\pm$ 17 pA (Figures 3B, 3C, and 3D, n = 5). We found that the latency between onset of vertical indentation and current activation was about 70 $\pm$ 20 ms with a specific threshold of 18 $\pm$ 4 pN (Figures 3B and 3C). The mechanosensitive currents were slowly inactivating with a time constant of inactivation of about 200 ms. To further verify the minimal threshold for the inward current, we applied single low-force mechanical stimuli (K = 0.046 pN/nm and F = 13 $\pm$ 1 pN). As expected, the inward current was relatively rare (10% of the stimulated neurons). However, the average peak current was reduced with an amplitude of 18 $\pm$ 5 pA (Figure 3E).

Taken together, these results suggest that the mechanically evoked response of hippocampal neurons requires extracellular calcium entry from the extracellular space through transmembrane ion channels.

Presence of mechanosensitive channels in hippocampal neurons

We examined whether canonical mechanosensitive channels, such as Piezo1 and Piezo2, were endogenously expressed in hippocampal cultures by immunohistochemistry. To address this, neuronal culture at 2 DIV were double stained with antibodies to TuJ1, a neuron-specific class III b-tubulin. Colocalization with TuJ1 staining revealed that Piezo1 is highly expressed in neurons (Figure 4A), while Piezo2 in glial cells (Figure 4B); indeed, TuJ-1 staining failed to colocalize with staining for Piezo2 (Figures 4A and 4B).

The molecular cascade initiated by mechanical stimuli

Next, we decided to identify the potential biomolecular cascade initiated by the entry of calcium ions through MSCs. Several molecular cascades initiated by an elevation of $[Ca^{2+}]_i$ involve the activation

of CaMKII and of small GTPases as long-term potentiation in synapses and spines (Hell, 2014; Murakoshi et al., 2011; Hedrick and Yasuda, 2017). Recent data suggest that a crosstalk may exist between Ca^{2+} mechanically activated signaling and Rho GTPase signaling. In fact, in the mechanotransduction context, it has been documented that RhoA is a central downstream effector in various kinds of cells (Chronopoulos et al., 2020; Pardo-Pastor et al., 2018; Keung et al., 2011). Initially, we investigated the potential activation of the mechanically evoked CaMKII using the intramolecular Camuiα-CR FRET sensor (Lam et al., 2012). In this sensor, CAMKII was doubly tagged with green fluorescent protein (GFP, donor) and mRuby2 (acceptor), which are close when CAMKII is inactive; therefore, FRET occurs when CAMKII is not active.

Following the activation of CaMKII, GFP and mRuby2 are separated, leading to a decrease in the FRET signal. Images of the donor and acceptor, i.e., of fluorescence emitted by GFP and mRuby2 (Figure 5B), were captured 48h post transfection using a dual-sensor CCD. We measured the ratio of GFP/mRuby2 fluorescence, which was correlated with the activation levels of CAMKII (Figure 5B). When this ratio was stable, we applied a mechanical stimulation composed of three pulses with a stiffness of 0.14 pN/nm. Averaged data from seven experiments indicated that CAMKII was activated by mechanical stimulation with a peak of 0.08 $\pm$ 0.04 and with a latency of 1.7 $\pm$ 1.2 s, as shown in Figures 5C and 5D. In total, 35% of the neurons show CAMKII activation to the repetitive mechanical indentation. We repeated similar FRET experiments to probe the activation of small G protein RhoA. In this case, we transfected hippocampal neurons with the Raichu-RhoA-CR sensor (Lam et al., 2012) (Figures 5E and 5F).

This intramolecular FRET probe is doubly tagged with green fluorescent protein (GFP, donor) attached to the PKN RhoA-binding domain and mRuby2 (acceptor) (Figure 5F) attached to RhoA-GDP, and the activation of RhoA is signaled by an increase in FRET. Therefore, the activation of CAMKII is indicated by a decrease in FRET (increase in D/A), while the activation of RhoA is indicated by an increase in FRET (increase in A/D). From the images of the donor and acceptor, i.e., of fluorescence emitted by GFP and mRuby2 (Figure 5E), we measured the ratio of fluorescence A/D (Figure 5F) following mechanical stimulation using the same parameters of the CAMKII experiments. This ratio before mechanical stimulation was used as a baseline reference. The repetitive mechanical stimulation (3 pulses, 1Hz, and k: 0.14 pN/nm) evoked a clear increase in A/D with a value of 0.04 $\pm$ 0.012 and a delay of approximately 18.5 $\pm$ 3.7 s (Figures 5G and 5H, n = 4) in 30% of the stimulated neurons. These results suggest that low picoNewton force applied vertically to plasma membrane of hippocampal neurons activates a biochemical cascade involving the CAMKII and the small G protein RhoA.

Growth cones respond to mechanical stimulation

Next, we investigate the growth cone (GC) hippocampal response to low picoNewton forces vertically applied. To test this possibility, we first searched for GCs that had filopodia actively moving and exploring the surrounding environment. GCs from hippocampal neurons moving vigorously were routinely found in the dish, and when a GC was active for at least 5 min, a polystyrene bead trapped in the equilibrium position of the laser beam of the OT was moved above it (Figure 6A). Bright field images of the moving GC were acquired for at least 5 min at 5 Hz and then, using a trap stiffness of 0.14 pN/nm an indentation consisting of three to six mechanical stimuli was applied. During mechanical stimulation, bright field images were acquired at 5 Hz for approximately 3 min (Figure 6B), and the length and orientation of the filopodium were measured and quantified (Figures 6C and 6D). The collected data showed that three repetitive stimuli evoked retraction/turning in approximately 50% of the stimulated GCs.

We observed a retraction of 1.7 $\pm$ 0.2 μm (single red arrow in Figure 6B) and a turning with a mean of angle of 7.5 $\pm$ 4.5 (Figures 6C and 6D, n = 12). Whereas, six mechanical stimuli evoked a retraction of 1.6 $\pm$ 0.4 μm (single red arrow in Figures 6B and 6D, n = 10) and a turning with a mean angle of 28.0 $\pm$ 4.7 (Figure 6C) in almost 80% of the stimulated GCs (Video S1). We conclude that hippocampal neurons respond to very low mechanical stimuli reminiscent to what is observed when a chemo-repellent agent is focally applied, i.e., exhibiting retraction/turning. These results are in agreement with previous studies in which the application of tension to neurites may also lead to their retraction (Franze et al., 2009; Dennerll et al., 1988). Furthermore, it has been shown that extracellular matrix molecules that inhibit MSC activity in sensory neurons also modulate the behavior of growth cones (Chiang et al., 2011) leading to increased branching of sensory terminals.

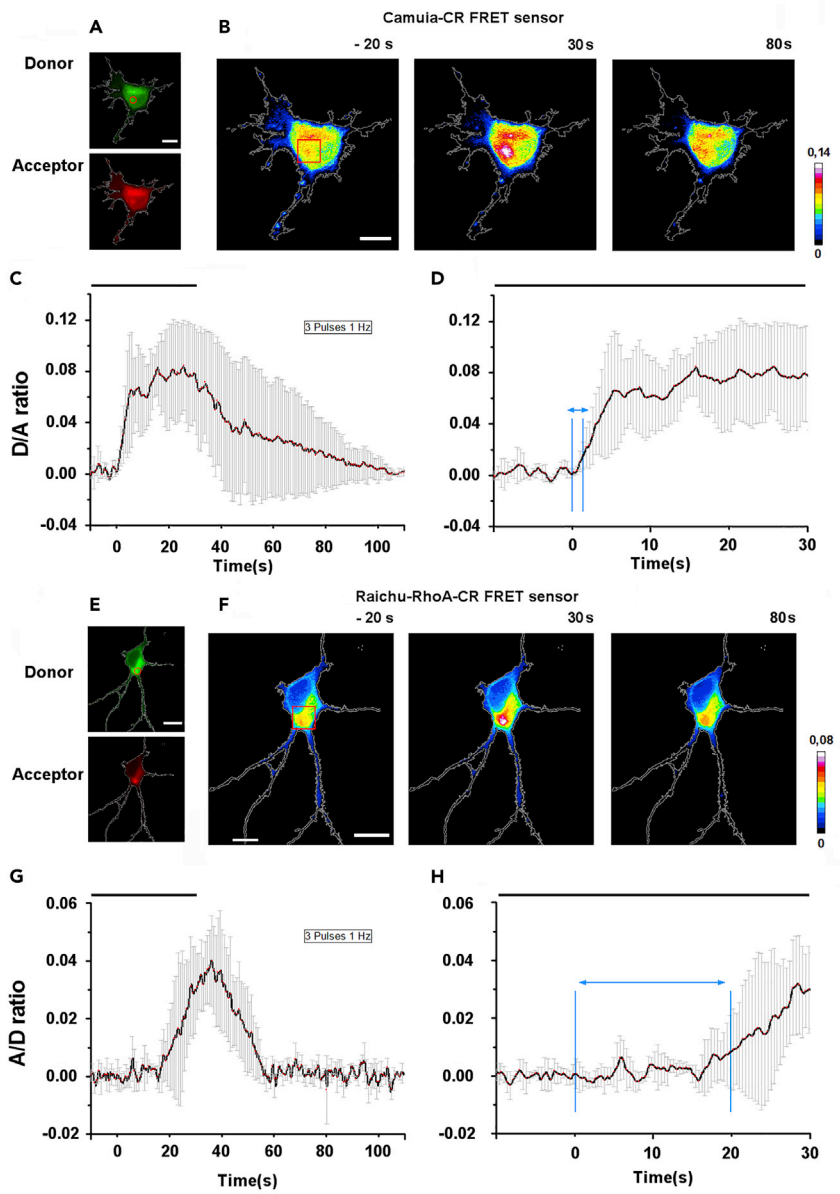

Figure 5. The activation of CAMKII and RhoA by mechanical stimulation

(A) Fluorescence images of the donor and acceptor used for the FRET measurement for the detection of CAMKII activation (The red circle indicates the site of mechanical stimulation). Scale bar, 10 μm.

(B) Ratiometric images (D/A ratio) before and after (−30 and 80 s) mechanical stimulation. The red square is the ROI used to compute the FRET signal. Scale bar, 10 μm.

(C) Time course of the FRET signal for the activation of CAMKII averaged from three experiments. The time zero indicates the mechanical stimulation (three pulses with high-force regime).

(D) Enlargement of C for t = −10 s:30 s.

(E) Fluorescence images of the donor and acceptor used for the FRET measurement for the detection of RhoA activation. The red circle indicates the site of mechanical stimulation. Scale bar, 10 μm.

(F) Ratiometric images (A/D ratio) before and after (30 and 80 s) stimulation with one ROI used to compute the FRET signal. Scale bar, 10 μm.

(G). Statistical analysis of RhoA activation (n = 5).

(H) As in (D) but for RhoA experiments (n = 4). Data are represented as mean ± SD.

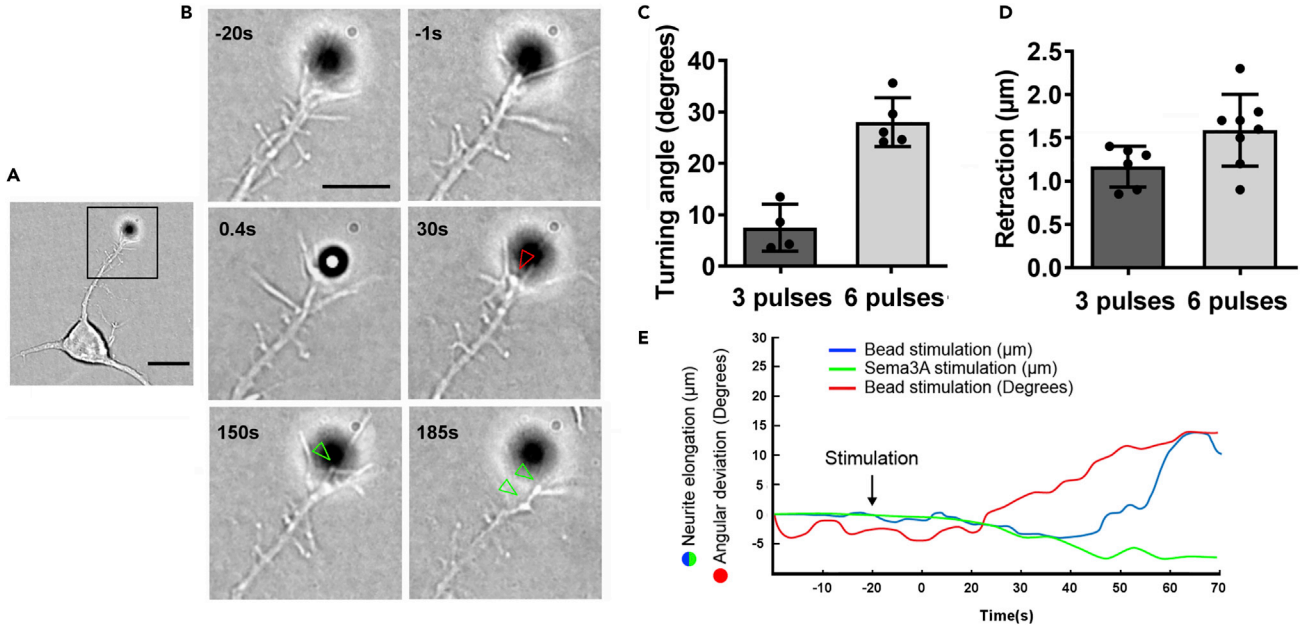

Figure 6. Response of hippocampal GC to mechanical stimulation

(A) Bright-field image of hippocampal neurons and a trapped bead near the GC (black square). Scale bar, 10 µm.

(B) Time course of GC response under repetitive mechanical stimulation (6 pulses, time= 0s) with retraction (red arrow, t= 30s) and turning (green arrows, t=150s and 185s). Scale bar, 5 µm.

(C) Relation between the amplitude of the turning angle and the number of applied pulses. The turning angles were determined by measuring the angle between the GC's initial trajectory and the final trajectory of that GC after mechanical stimulation.

(D) Relationship between the retraction of GC and the number of applied pulses.

(E) Tracking of the GC over time; blue indicates neurite elongation before and after bead stimulation (black arrow); green indicates neurite elongation before and after Sema3A administration (black arrow); red indicates angular deviation before and after bead stimulation (black arrow). The data for the effect of Sema3A administration were redrawn from Pinato et al. (2012). Data in (C and D) are represented as mean ± SD.

Mechanical signaling during the formation of neuronal networks

Subsequently, we wanted to verify that if mechanosignaling plays a role during the formation of neuronal networks, their connectivity would be altered when MCSs are blocked. To test this possibility, we cultured dissociated hippocampal neurons for seven days in control conditions (Figure 7A) and in the presence of 10-µM GsMTx-4 and, after fixation, we analyzed the immunostaining for Actin (green), Tubulin (red) and DAPI (blue). When the localization of nuclei was considered visualizing only the DAPI staining, visual inspection showed that following blockage of MSCs, neurons were more interspersed (compare panels of Figure 7B). For statistical confirmation, we performed a clustering analysis of the DAPI spots. We used the clustering method (Rodriguez and Laio, 2014) in which cluster centers are identified as local density maxima that are far away from any points of higher density. We computed the histogram of the fraction of cells forming a cluster and we verified that, in control conditions, the mean fraction of clustered cells was 47%, which was higher than that in the presence of GsMTx-4, i.e., 30%. We also computed the cluster entropy (Figure 7B, upper panel).We found that, in control conditions, this quantity was 0.96 ± 0.4, but in the presence of the inhibitor of MSCs increased to 1.32 ± 0.25 (two-sample Kolmogorov-Smirnov p = 0.03), indicating a lower degree of cluster formation. The plot of the relation between cluster entropy versus the fraction of clustered cells (Figure 7B, lower panel) shows that data from control conditions are statistically separated from those obtained in the presence of the inhibitor (two-sample Kolmogorov-Smirnov p = 0.03).

Next, we investigated how GsMTx-4 influences the synapse formation. We performed immunofluorescence of PSD-95 and VGlut1 on dissociated hippocampal neurons cultured for seven days in control conditions and in the presence of 10-µM GsMTx-4, and after fixation (Figure S1). We used the Pearson's value to determine the correlation between the two staining and we found that in control conditions the value is 0.67 ± 0.1 and with GsMTx-4 is 0.58 ± 0.11. This indicates that the synaptic abundancy is higher in control conditions and that with 10 µM GsMTx-4 the synaptic presence is reduced by 14%.

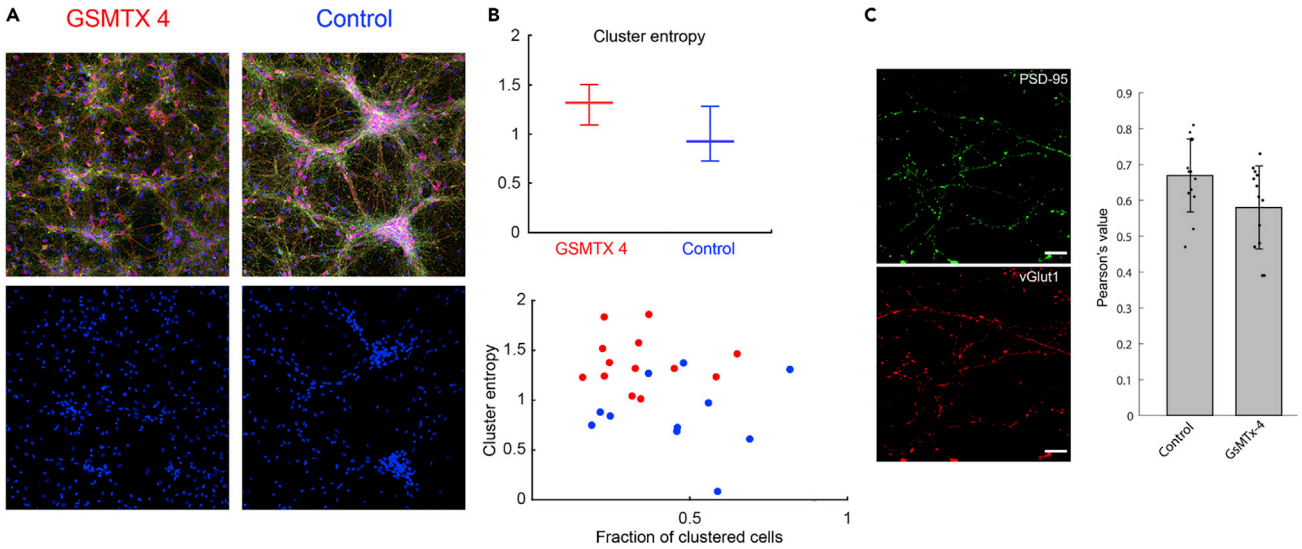

Figure 7. Forces during the formation of neuronal networks

(A) Immunostaining of hippocampal culture 7 days *in vitro*, with GsMTx-4 and in control condition. Actin is in green, tubulin in red and DAPI in blue.

(B) Cluster entropy computed on DAPI staining of neurons 7 days *in vitro* (upper panel) and relationship between cluster entropy versus the fraction of clustered cells (bottom panel).

(C) Immunofluorescence of dissociated hippocampal neurons after 7 days *in vitro* showing in green the PSD-95 (upper panel), in red VGlut1 (bottom panel). Pearson's values of the correlation of PSD-95 and VGlut1 was calculated in control conditions and with 10-μM GsMTx-4 (right panel). Data in (B and C) are represented as mean ± SD.

Therefore, we conclude that the inhibition of MSCs reduced the formation of synaptic structures *in vitro* suggesting a role for mechanosensitivity in the formation of neuronal networks of hippocampal cultures.

DISCUSSION

In the present manuscript, we studied the response of hippocampal neurons to localized mechanical indentation at low picoNewton forces. Previously, the response of central neurons to localized mechanical stimulation has been described using high forces (above 50 nN). In this study, the forces were in the range of 5–50 pN, which are dramatically smaller than the one applied in the previous techniques.

Using NG108-15 cells, we recently demonstrated that a single localized mechanical indentation in the range of 7.2 ± 1.5 pN cells evokes a local and transient calcium response of 0.0326 ± 0.004 (DF/F) (Falleroni et al., 2018). This manuscript shows that hippocampal neurons are sensitive to slightly higher mechanical forces. In fact, to evoke similar changes in $[Ca^{2+}]_i$, we used a trap stiffness of k = 0.14 pN/nm, which was four times larger than the one used with NG108-15 cells (k = 0.035 pN nm^{-1}). This difference could be attributed to differences between cells in the biochemical composition of the plasma membrane and in the local cytoskeleton. Interestingly, the NG108-15 cells lack endogenous caveolins, which are the major structural proteins of glycolipid/cholesterol-rich flask-shape invaginations at the plasma membrane, called caveolae (Gorodinsky and Harris, 1995). Differently, caveolin is well expressed in many cell types, including hippocampal neurons. It binds cholesterol and also increases the trafficking of cholesterol from endoplasmic reticulum to plasma membrane (Williams and Lisanti, 2004). Elevation of the membrane cholesterol level alters the mechanical properties of the membrane bilayer, resulting in increased membrane stiffness and, consequently, in increased energy associated with channels opening (Toselli et al., 2005).

Similar to that observed in the NG108-15 cells, repetitive mechanical stimulation induced a more sustained and variable calcium response. In fact, the initial (within 200 ms from the mechanical stimulation) and small calcium increase was followed by a larger and global change reaching its DF/F peak in approximately 20 s. Moreover, we observed that the amplitude of the mechanically evoked calcium transient scales with both the applied force and the number of mechanical stimulations.

The molecular mechanisms of mechanosensitivity and mechanotransduction are in the process of being elucidated and two main mechanisms have emerged. Mechanosensing can occur in biological systems according to the so-called switch-like manner (Hoffman et al., 2011; Brierley, 2010) in which the mechanical forces are transmitted to cellular structures inducing conformation changes in specific proteins. This pathway occurs through the activation receptors of the family of integrins and cadherins, which are coupled on one side to the extracellular matrix and to the surrounding environment and, on the other side, to the cytoskeleton and to the actomyosin complex (Park et al., 2020).

It has been demonstrated that cell adhesion molecules such as cadherin and talin (Charras and Yap, 2018; Del Rio et al., 2009) or integrins receptors are sensitive to forces below 30 pN (Jurchenko et al., 2014; Kong et al., 2009). The other mechanism underlying mechanotransduction occurs through the activation of MSCs. Because MSCs are mostly cation permeable, the concomitant entry of Ca^{2+} ions into the cell may be responsible for activating the transduction pathway (Murata et al., 2014; Han et al., 2012). Using chemical perturbation (treatment with BAPTA and GsMT-x 4), we found that the mechanically evoked response of hippocampal neurons requires the entry of extracellular calcium from the extracellular space through transmembrane ion channels. Interestingly, treatment with GsMTx-4 reduced the amplitude of calcium transients in 40% of mechanically stimulated neurons (Figure 2D). These results suggest that the mechanically evoked calcium response in hippocampal neurons appears to be partially mediated by canonical MSCs in the plasma membrane, in agreement with previous studies establishing that a number of neuronal structures not conventionally described as mechanosensitive channel can be mechanically modulated (Tyler, 2012).

We confirmed the presence of mechanosensitive channels (MSCs), such as Piezo1, in hippocampal neurons by immunochemistry. Recently, discovered mechanosensitive Piezo channels emerged as the main molecular detectors of mechanical forces in different kind of cells (Richardson et al., 2021). New insights of Piezo1 structure by cryo-EM (Guo and MacKinnon, 2017) suggest that this channel might sense membrane tension through changes in the local curvature of the membrane (Liang and Howard, 2018). Thus, the membrane tension will alter gating energetics in proportion to the change in the gating-associated area, leading to a higher sensitivity of gating.

In their canonical forms, Piezo channels inactivate rapidly following mechanical stimulation with a time constant less than 50 ms (Coste et al., 2010). However, there are several additional cellular components that can influence Piezo1 kinetics to mechanical stimuli (Shi et al., 2020; Peyronnet et al., 2013). We found that the inward mechanosensitive current was slow inactivating with a time constant of inactivation of about 200 ms. Notably, multiple cell lines exhibit a slow-inactivating mechanosensitive current that is attributable to Piezo1, such as mouse embryonic stem cells or mouse C2C12 cells (del Marmol et al., 2018; Coste et al., 2010). It has been described that there are multiple mechanisms that can tune sensitivity of Piezo1, including both changes in the lipid environment (Ridone et al., 2020; Gottlieb et al., 2012) and interacting protein partners (Qi et al., 2015; Cox et al., 2016; Bavi et al., 2019; Poole et al., 2014).

We found an inward current mechanically evoked with an average amplitude of of 75 $\pm$ 17 pA (Figures 3B and 3E) on hippocampal neuron stimulated with the high-force regime. In these experiments, the latency between onset of vertical indentation and current activation was about 70 $\pm$ 20 ms with a specific threshold of 18 $\pm$ 4 pN (Figures 3B and 3C). To further verify the minimal threshold for the inward current, we applied single low-force mechanical stimuli (K = 0.046 pN/nm and F = 13 $\pm$ 1 pN). As expected, the inward current was relatively rare (10% of the stimulated neurons). However, the average peak current was reduced with an amplitude of 17 $\pm$ 5 pA (Figure 3E).

Considering a minimum force F = 13 pN and a displacement x = 280 nm, the work done by the bead is about L = 1820 pN nm $\sim$ 444 K_BT. This energy can be transferred to the cell membrane and the MSC in different ways, inducing MSC deformation during transition between closed and open states (Markin and Sachs, 2004) including changes of area, shape and length. The barrier energy between the two states is of the order of 10–20 K_BT. Although only a part of the work done by the trapped bead is effective to induce MSC activation, for a 20% efficiency we estimate between four and eight MSC can be activated with a force F = 13 pN. The indentation parameter (S), when less than 500 nm, can be related to the force (F) exerted on the bead (which is equal to the force exerted by the bead on the cell) by a proportionality factor, k: F = k *S, where k is the elastic constant or stiffness of the trap. As a consequence, we obtained an average

indentation value of 280 ± 12 nm at low-force and a value of 360 ± 18 at high-force regime. Besides force component, the indentation value could play a key role on the mechanoresponse. For example, there have been studies showing that for MSC activation, the relevant parameter could be the magnitude of deflection rather than the magnitude of force (Petzold et al., 2013; Bavi et al., 2019).

When a low localized picoNewton mechanical stimulus is applied vertically, the neuron feels the combined effect of a force and of the concomitant indentation of its plasma membrane. As a consequence, transmembrane channels open inducing a fast increase in $[Ca^{2+}]_i$ (Figure 1). This localized calcium entry diffuses inside the neuron and is likely to activate several signaling pathways and most likely an additional release of calcium from the intracellular store (see the delayed and slower rise of $[Ca^{2+}]_i$ in Figures 1 and 2). Combining data obtained with the fluorescent calcium indicator Fluo-4, FRET measurements for the activation of CamKII and RhoA and experiments with fluorescently labeled actin, we have elucidated some steps of this biochemical cascade. The elevation of $[Ca^{2+}]_i$ activates CAMKII within 1–5 s, which in turn potentially activates the small GTPase RhoA within 10–20 s.

The biochemical cascade initiated by weak mechanical forces is similar to what has already been described in spines (Murakoshi et al., 2011). In these experiments, a brief transient Ca^{2+} pulse causes a rapid activation of CaMKII within approximately 0.5 s, which decays in approximately 10 s. In hippocampal neurons, CAMKII activation occurs in a similar time window, but CAMKII remains activated for a longer time, presumably because of a longer elevation of $[Ca^{2+}]_i$. The activation of CAMKII terminates with a delay of 10–20 s following the return of $[Ca^{2+}]_i$ to its resting. In spines, long-term plasticity initiated by a rapid pulse of glutamate and the associated increase in $[Ca^{2+}]_i$ activate RhoA and Cdc42 with a delay of some seconds (Hedrick and Yasuda, 2017), similar to what was observed in hippocampal neurons. Additionally, in spines and in other preparations, cytoskeletal reorganization occurs on a timescale of minutes (Nakahata and Yasuda, 2018).

It is well established that mechanosensing and tissue stiffness control migration, axon growth during morphogenesis and neuronal development (Koser et al., 2016; Barriga et al., 2018). These studies show that the MCS channel Piezo1 has a major role in aging and development, and it is likely that the activation of Piezo1 initiates a biochemical cascade similar to that described here.

Our results showed that neurons of the CNS, such as hippocampal neurons, are sensitive to mechanical forces in the range of forces exerted by hippocampal filopodia and lamellipodia. Therefore, in neuronal networks, in addition to the usual electrical and chemical signaling, mechanical signaling is present. Low picoNewton mechanical stimulation on growth cones (GCs) acts as repulsive stimuli inducing turning and retraction (Figure 7). These results are in agreement with previous studies, in which the application of tension to neurites may also lead to their retraction (Franze et al., 2009; Dennerll et al., 1988). Furthermore, it has been shown that extracellular matrix molecules that inhibit MSC activity in sensory neurons also modulate the behavior of growth cones (Chiang et al., 2011), leading to increased branching of sensory terminals.

When a GC encounters the soma of another neuron, it is likely to evoke an increase in $[Ca^{2+}]$i. We propose that the formation of neuronal networks requires the processing of concomitant mechanical, chemical and electrical signals, giving rise to a complex mechanical computation (Laishram et al., 2009), as suggested by the reduction of the formation of synaptic structures when MCSs are inhibited (Figure 7). GCs located at the tip of neurites explore the environment and decode all the encountered mechanical, electrical and chemical clues and then "decide/compute" what to do. Mechanical computation represents the functional understanding of mechanosensitivity and mechanotransduction described in the present article; it aims at unraveling the strategy used by filopodia and lamellipodia during their exploration and navigation, and the mechanical problems that neurons need to solve during development and aging in the adult brain.

In the adult and fully developed brain, some neurons navigate in the dense tissue and new synapses are formed and therefore neurons, dendrites and spines are not immobile and exert forces on the surrounding cells. Live cell imaging of microglia and of adult stem cells (Ormel et al., 2018) shows that these cells move in the dense tissue almost as fast as when they are dissociated and examined in conventional Petri dish. Understanding the molecular and biophysical mechanism of how cells process concomitant mechanical

and chemical signals and regulate their response will clarify how cells change shape and control their migratory behavior. Therefore, mechanical signaling among cells is important and ubiquitous, but still needs to be better clarified.

Limitations of the study

Our present results indicate that the application of a force in the range of 13–50 pN by plasma membrane indentation results in an influx of intracellular calcium from the extracellular space through transmembrane ion channels. Treatment with Gsmtx4 suggests that the response is partially mediated by canonical mechanosensory channels. Therefore, it would be interesting to analyze the response to calcium by using various chemical compounds to inhibit several transmembrane channels not conventionally described as mechanosensitive channels, including voltage-gated sodium channels and voltage-gated potassium channels.

In addition, we observed a mechano-dependent activation of CAMKII and the small G protein RhoA. It would be interesting to use inhibition strategies to analyze whether there is a direct signaling module between CAMKII and RhoA following mechanical stimulation at a low-force regime, as suggested by the timing of activation observed in this study.

STAR★METHODS

Detailed methods are provided in the online version of this paper and include the following:

- KEY RESOURCES TABLE
- RESOURCE AVAILABILITY
  - Lead contact
  - Materials availability
  - Data and code availability
- EXPERIMENTAL MODEL AND SUBJECT DETAILS
  - Hippocampal neuronal culture
- METHOD DETAILS
  - Calcium imaging experiment
  - Optical manipulation
  - Force and indentation measurement
  - Electrophysiology
  - Immunofluorescence analysis
  - FRET measurements
- QUANTIFICATION AND STATISTICAL ANALYSIS
- ADDITIONAL RESOURCES

SUPPLEMENTAL INFORMATION

Supplemental information can be found online at https://doi.org/10.1016/j.isci.2022.103807.

ACKNOWLEDGMENTS

We thank Beatrice Pastore, Marco Gigante and Fabrizio Manzino for technical assistance; Rossella Gorgoglione for carefully reading the manuscript and Jelena Ban for thought provoking discussions that inspired this study.

AUTHOR CONTRIBUTIONS

FF, VT, and DC contributed to the conception and design of the study. FF and YL designed, conducted, and analyzed *in vitro* calcium experiments. FF and UB conducted and analyzed the optical tweezer and electrophysiology experiments. ZY performed immunofluorescence experiments. FF and YL designed, conducted and analyzed *in vitro* FRET experiments. SM performed and analyzed the experiments concerning the mechanical signaling during the formation of neuronal networks. FF, VT, and DC wrote the manuscript.

DECLARATION OF INTERESTS

The authors declare no competing interests.

Received: April 14, 2021
Revised: September 21, 2021
Accepted: January 20, 2022
Published: February 18, 2022

REFERENCES

Amin, L., Ercolini, E., Ban, J., and Torre, V. (2013). Comparison of the force exerted by hippocampal and DRG growth cones. PLoS One *8*, e73025. https://doi.org/10.1371/journal.pone.0073025.

Barriga, E.H., Franze, K., Charras, G., and Mayor, R. (2018). Tissue stiffening coordinates morphogenesis by triggering collective cell migration in vivo. Nature *554*, 523–527. https://doi.org/10.1038/nature25742.

Bavi, N., Richardson, J., Heu, C., Martinac, B., and Poole, K. (2019). PIEZO1-Mediated currents are modulated by substrate mechanics. ACS Nano *13*, 13545–13559. https://doi.org/10.1021/acsnano.9b07499.

Brierley, S.M. (2010). Molecular basis of mechanosensitivity. Auton. Neurosci. *153*, 58–68. https://doi.org/10.1016/j.autneu.2009.07.017.

Charras, G., and Yap, A.S. (2018). Tensile forces and mechanotransduction at cell–cell junctions. Curr. Biol. *28*, R445–R457. https://doi.org/10.1016/j.cub.2018.02.003.

Chiang, L.-Y., Poole, K., Oliveira, B.E., Duarte, N., Sierra, Y.A., Bruckner-Tuderman, L., Koch, M., Hu, J., and Lewin, G.R. (2011). Laminin-332 coordinates mechanotransduction and growth cone bifurcation in sensory neurons. Nat. Neurosci. *14*, 993–1000. https://doi.org/10.1038/nn.2873.

Chronopoulos, A., Thorpe, S.D., Cortes, E., Lachowski, D., Rice, A.J., Mykuliak, V.V., Róg, T., Lee, D.A., Hytönen, V.P., and Del Río Hernández, A.E. (2020). Syndecan-4 tunes cell mechanics by activating the kindlin-integrin-RhoA pathway. Nat. Mater. *19*, 669–678. https://doi.org/10.1038/s41563-019-0567-1.

Cojoc, D., Difato, F., Ferrari, E., Shahapure, R.B., Laishram, J., Righi, M., Di Fabrizio, E.M., and Torre, V. (2007). Properties of the force exerted by filopodia and lamellipodia and the involvement of cytoskeletal components. PLoS One *2*, e1072. https://doi.org/10.1371/journal.pone.0001072.

Coste, B., Mathur, J., Schmidt, M., Earley, T.J., Ranade, S., Petrus, M.J., Dubin, A.E., and Patapoutian, A. (2010). Piezo1 and Piezo2 are essential components of distinct mechanically activated cation channels. Science *330*, 55–60. https://doi.org/10.1126/science.1193270.

Cox, C.D., Bae, C., Ziegler, L., Hartley, S., Nikolova-Krstevski, V., Rohde, P.R., Ng, C.A., Sachs, F., Gottlieb, P.A., and Martinac, B. (2016). Removal of the mechanoprotective influence of the cytoskeleton reveals PIEZO1 is gated by bilayer tension. Nat. Commun. *7*, 10366. https://doi.org/10.1038/ncomms10366.

Dennerll, T.J., Joshi, H.C., Steel, V.L., Buxbaum, R.E., and Heidemann, S.R. (1988). Tension and compression in the cytoskeleton of PC-12 neurites. II: quantitative measurements. J. Cell Biol. *107*, 665–674. https://doi.org/10.1083/jcb.107.2.665.

del Rio, A., Perez-Jimenez, R., Liu, R., Roca-Cusachs, P., Fernandez, J.M., and Sheetz, M.P. (2009). Stretching single talin rod molecules activates vinculin binding. Science *323*, 638–641. https://doi.org/10.1126/science.1162912.

Dogterom, M., and Yurke, B. (1997). Measurement of the force-velocity relation for growing microtubules. Science *278*, 856–860. https://doi.org/10.1126/science.278.5339.856.

Falleroni, F., Torre, V., and Cojoc, D. (2018). Cell mechanotransduction with piconewton forces applied by optical tweezers. Front. Cell Neurosci. *12*, 130. https://doi.org/10.3389/fncel.2018.00130.

Footer, M.J., Kerssemakers, J.W., Theriot, J.A., and Dogterom, M. (2007). Direct measurement of force generation by actin filament polymerization using an optical trap. Proc. Natl. Acad. Sci. U S A *104*, 2181–2186. https://doi.org/10.1073/pnas.0607052104.

Franze, K., Gerdelmann, J., Weick, M., Betz, T., Pawlizak, S., Lakadamyali, M., Bayer, J., Rillich, K., Gögler, M., Lu, Y.B., et al. (2009). Neurite branch retraction is caused by a threshold-dependent mechanical impact. Biophysical J. *97*, 1883–1890. https://doi.org/10.1016/j.bpj.2009.07.033.

Gaub, B.M., Kasuba, K.C., Mace, E., Strittmatter, T., Laskowski, P.R., Geissler, S.A., Hierlemann, A., Fussenegger, M., Roska, B., and Müller, D.J. (2020). Neurons differentiate magnitude and location of mechanical stimuli. Proc. Natl. Acad. Sci. U S A *117*, 848–856. https://doi.org/10.1073/pnas.1909933117.

Gnanasambandam, R., Ghatak, C., Yasmann, A., Nishizawa, K., Sachs, F., Ladokhin, A.S., Sukharev, S.I., and Suchyna, T.M. (2017). GsMTx4: mechanism of inhibiting mechanosensitive ion channels. Biophysical J. *112*, 31–45. https://doi.org/10.1016/j.bpj.2016.11.013.

Gorodinsky, A., and Harris, D.A. (1995). Glycolipid-anchored proteins in neuroblastoma cells form detergent-resistant complexes without caveolin. J. Cell Biol. *129*, 619–627. https://doi.org/10.1083/jcb.129.3.619.

Gottlieb, P.A., Bae, C., and Sachs, F. (2012). Gating the mechanical channel Piezo1: a comparison between whole-cell and patch recording. Channels *6*, 282–289. https://doi.org/10.4161/chan.21064.

Guo, Y.R., and MacKinnon, R. (2017). Structure-based membrane dome mechanism for Piezo mechanosensitivity. eLife *6*, e33660. https://doi.org/10.7554/eLife.33660.

Han, S.-K., Wouters, W., Clark, A., and Herzog, W. (2012). Mechanically induced calcium signaling in chondrocytes in situ: mechanically induced calcium signals in chondrocytes in situ. J. Orthop. Res. *30*, 475–481. https://doi.org/10.1002/jor.21536.

Hedrick, N.G., and Yasuda, R. (2017). Regulation of Rho GTPase proteins during spine structural plasticity for the control of local dendritic plasticity. Curr. Opin. Neurobiol. *45*, 193–201. https://doi.org/10.1016/j.conb.2017.06.002.

Hell, J.W. (2014). CaMKII: claiming center stage in postsynaptic function and organization. Neuron *81*, 249–265. https://doi.org/10.1016/j.neuron.2013.12.024.

Hoffman, B.D., Grashoff, C., and Schwartz, M.A. (2011). Dynamic molecular processes mediate cellular mechanotransduction. Nature *475*, 316–323. https://doi.org/10.1038/nature10316.

Jia, Y., Zhao, Y., Kusakizako, T., Wang, Y., Pan, C., Zhang, Y., Nureki, O., Hattori, M., and Yan, Z. (2020). TMC1 and TMC2 proteins are pore-forming subunits of mechanosensitive ion channels. Neuron *105*, 310–321.e3. https://doi.org/10.1016/j.neuron.2019.10.017.

Jurchenko, C., Chang, Y., Narui, Y., Zhang, Y., and Salaita, K.S. (2014). Integrin-generated forces lead to streptavidin-biotin unbinding in cellular adhesions. Biophys. J. *106*, 1436–1446. https://doi.org/10.1016/j.bpj.2014.01.049.

Keung, A.J., de Juan-Pardo, E.M., Schaffer, D.V., and Kumar, S. (2011). Rho GTPases mediate the mechanosensitive lineage commitment of neural stem cells. Stem Cell *29*, 1886–1897. https://doi.org/10.1002/stem.746.

Kong, F., García, A.J., Mould, A.P., Humphries, M.J., and Zhu, C. (2009). Demonstration of catch bonds between an integrin and its ligand. J. Cell Biol. *185*, 1275–1284. https://doi.org/10.1083/jcb.200810002.

Koser, D.E., Thompson, A.J., Foster, S.K., Dwivedy, A., Pillai, E.K., Sheridan, G.K., Svoboda, H., Viana, M., Costa, L.D., Guck, J., et al. (2016). Mechanosensing is critical for axon growth in the developing brain. Nat. Neurosci. *19*, 1592–1598. https://doi.org/10.1038/nn.4394.

Laishram, J., Avossa, D., Shahapure, R., and Torre, V. (2009). Mechanical computation in neurons. Dev. Neurobiol. *69*, 731–751. https://doi.org/10.1002/dneu.20733.

Lam, A.J., St-Pierre, F., Gong, Y., Marshall, J.D., Cranfill, P.J., Baird, M.A., McKeown, M.R., Wiedenmann, J., Davidson, M.W., Schnitzer, M.J., et al. (2012). Improving FRET dynamic range with bright green and red fluorescent proteins. Nat. Methods *9*, 1005–1012. https://doi.org/10.1038/nmeth.2171.

Liang, X., and Howard, J. (2018). Structural biology: Piezo senses tension through curvature. Curr. Biol. *28*, R357–R359. https://doi.org/10.1016/j.cub.2018.02.078.

Lumpkin, E.A., and Caterina, M.J. (2007). Mechanisms of sensory transduction in the skin. Nature *445*, 858–865. https://doi.org/10.1038/nature05662.

Markin, V.S., and Sachs, F. (2004). Thermodynamics of mechanosensitivity. Phys. Biol. *1*, 110–124. https://doi.org/10.1088/1478-3967/1/2/007.

del Mármol, J.I., Touhara, K.K., Croft, G., MacKinnon, R., et al. (2018). Piezo1 forms a slowly-inactivating mechanosensory channel in mouse embryonic stem cells. eLife *7*, e33149. https://doi.org/10.7554/eLife.33149.

Marshall, K.L., and Lumpkin, E.A. (2012). The molecular basis of mechanosensory transduction. In Sensing in Nature, C. López-Larrea, ed. (Springer US (Advances in Experimental Medicine and Biology)), pp. 142–155. https://doi.org/10.1007/978-1-4614-1704-0_9.

Murakoshi, H., Wang, H., and Yasuda, R. (2011). Local, persistent activation of Rho GTPases during plasticity of single dendritic spines. Nature *472*, 100–104. https://doi.org/10.1038/nature09823.

Murata, N., Ito, S., Furuya, K., Takahara, N., Naruse, K., Aso, H., Kondo, M., Sokabe, M., and Hasegawa, Y. (2014). Ca^{2+} influx and ATP release mediated by mechanical stretch in human lung fibroblasts. Biochem. Biophys. Res. Commun. *453*, 101–105. https://doi.org/10.1016/j.bbrc.2014.09.063.

Nakahata, Y., and Yasuda, R. (2018). Plasticity of spine structure: local signaling, translation and cytoskeletal reorganization. Front. Synaptic Neurosci. *10*, 29. https://doi.org/10.3389/fnsyn.2018.00029.

Neuman, K.C., and Block, S.M. (2004). Optical trapping. Rev. Sci. Instr. *75*, 2787–2809. https://doi.org/10.1063/1.1785844.

Nikolaev, Y.A., Dosen, P.J., Laver, D.R., van Helden, D.F., and Hamill, O.P. (2015). Single mechanically-gated cation channel currents can trigger action potentials in neocortical and hippocampal pyramidal neurons. Brain Res *1608*, 1–13. https://doi.org/10.1016/j.brainres.2015.02.051.

Ormel, P.R., Vieira de Sá, R., van Bodegraven, E.J., Karst, H., Harschnitz, O., Sneeboer, M.A.M., Johansen, L.E., van Dijk, R.E., Scheefhals, N., Berdenis van Berlekom, A., et al. (2018). Microglia innately develop within cerebral organoids. Nat. Commun. *9*, 4167. https://doi.org/10.1038/s41467-018-06684-2.

Pardo-Pastor, C., Rubio-Moscardo, F., Vogel-González, M., Serra, S.A., Afthinos, A., Mrkonjic, S., Destaing, O., Abenza, J.F., Fernández-Fernández, J.M., Trepat, X., et al. (2018). Piezo2 channel regulates RhoA and actin cytoskeleton to promote cell mechanobiological responses. Proc. Natl. Acad. Sci. U S A *115*, 1925–1930. https://doi.org/10.1073/pnas.1718177115.

Park, J.S., Burckhardt, C.J., Lazcano, R., Solis, L.M., Isogai, T., Li, L., Chen, C.S., Gao, B., Minna, J.D., Bachoo, R., DeBerardinis, R.J., et al. (2020). Mechanical regulation of glycolysis via cytoskeleton architecture. Nature *578*, 621–626. https://doi.org/10.1038/s41586-020-1998-1.

Pathak, M.M., Nourse, J.L., Tran, T., Hwe, J., Arulmoli, J., Le, D.T., Bernardis, E., Flanagan, L.A., and Tombola, F. (2014). Stretch-activated ion channel Piezo1 directs lineage choice in human neural stem cells. Proc. Natl. Acad. Sci. U S A *111*, 16148–16153. https://doi.org/10.1073/pnas.1409802111.

Petzold, B.C., Park, S.J., Mazzochette, E.A., Goodman, M.B., and Pruitt, B.L. (2013). MEMS-based force-clamp analysis of the role of body stiffness in *C. elegans* touch sensation. Integr. Biol. *5*, 853–864. https://doi.org/10.1039/c3ib20293c.

Peyronnet, R., Martins, J.R., Duprat, F., Demolombe, S., Arhatte, M., Jodar, M., Tauc, M., Duranton, C., Paulais, M., Teulon, J., et al. (2013). Piezo1-dependent stretch-activated channels are inhibited by Polycystin-2 in renal tubular epithelial cells. EMBO Rep. *14*, 1143–1148. https://doi.org/10.1038/embor.2013.170.

Pinato, P., Cojoc, D., Lien, L.T., Ansuini, A., Ban, J., D'Este, E., and Torre, V. (2012). Less than 5 Netrin-1 molecules initiate attraction but 200 Sema3A molecules are necessary for repulsion. Sci. Rep. *675*. https://doi.org/10.1038/srep00675.

Poole, K., Herget, R., Lapatsina, L., Ngo, H.D., and Lewin, G.R. (2014). Tuning Piezo ion channels to detect molecular-scale movements relevant for fine touch. Nat. Commun. *5*, 3520. https://doi.org/10.1038/ncomms4520.

Qi, Y., Andolfi, L., Frattini, F., Mayer, F., Lazzarino, M., and Hu, J. (2015). Membrane stiffening by STOML3 facilitates mechanosensation in sensory neurons. Nat. Commun. *6*, 8512. https://doi.org/10.1038/ncomms9512.

Richardson, J., Kotevski, A., and Poole, K. (2021). From stretch to deflection: the importance of context in the activation of mammalian, mechanically activated ion channels. FEBS J. https://doi.org/10.1111/febs.16041.

Ridone, P., Pandzic, E., Vassalli, M., Cox, C.D., Macmillan, A., Gottlieb, P.A., and Martinac, B. (2020). Disruption of membrane cholesterol organization impairs the activity of PIEZO1 channel clusters. J. Gen. Physiol. *152*, e201912515. https://doi.org/10.1085/jgp.201912515.

Rodriguez, A., and Laio, A. (2014). Clustering by fast search and find of density peaks. Science *344*, 1492–1496. https://doi.org/10.1126/science.1242072.

Schneider, C.A., Rasband, W.S., and Eliceiri, K.W. (2012). NIH Image to ImageJ: 25 years of image analysis. Nat. Methods *9*, 671–675. https://doi.org/10.1038/nmeth.2089.

Shi, J., Hyman, A.J., De Vecchis, D., Chong, J., Lichtenstein, L., Futers, T.S., Rouahi, M., Salvayre, A.N., Auge, N., Kalli, A.C., et al. (2020). Sphingomyelinase disables inactivation in endogenous PIEZO1 channels. Cell Rep. *33*, 108225. https://doi.org/10.1016/j.celrep.2020.108225.

Toselli, M., Biella, G., Taglietti, V., Cazzaniga, E., and Parenti, M. (2005). Caveolin-1 expression and membrane cholesterol content modulate N-type calcium channel activity in NG108-15 cells. Biophys. J. *89*, 2443–2457. https://doi.org/10.1529/biophysj.105.065623.

Tyler, W.J. (2012). The mechanobiology of brain function. Nat. Rev. Neurosci. *13*, 867–878. https://doi.org/10.1038/nrn3383.

Williams, T.M., and Lisanti, M.P. (2004). [No title found]. Genome Biol. *5*, 214. https://doi.org/10.1186/gb-2004-5-3-214.

STAR★METHODS

KEY RESOURCES TABLE

REAGENT or RESOURCE	SOURCE	IDENTIFIER
Antibodies		
Anti-Piezo1 Antibody	Alomone labs	Cat#APC-087; RRID:AB_2756743
Anti-Piezo2 Antibody	Alomone labs	Cat#APC-090; RRID:AB_2876842
Anti-β-Tubulin III antibody	Sigma-Aldrich	Cat#T3952; RRID:AB_1841226
Biological samples		
Primary hippocampl neurons	Isolated from Wistar rats (P2)	N/A
Chemicals, peptides, and recombinant proteins		
GsMTx-4	Tocris	Cat#4912
BAPTA	Enzo life sciences	Cat#BML-CA412
Lipofectamine™ 3000	ThermoFisher	Cat#L3000001
Deposited data		
Data for the effect of Sema3A	Pinato et al. (2012)	N/A
Oligonucleotides		
pcDNA3- Camuiα -CR	Addgene	Cat#40256; RRID:Addgene_40256
pCAGGS-Raichu-RhoA-CR	Addgene	Cat#40258; RRID:Addgene_40258
Software and algorithms		
ImageJ	Schneider et al. (2012)	https://imagej.nih.gov/ij/
Prism	GraphPad Software	Prism - GraphPad
Clampfit	Molecular Devices	https://www.moleculardevices.com/
Origin	OriginLab Corporation	https://www.originlab.com/
dFoverFmovie	Github	https://gist.github.com/ackman678/5817461
Biosensor 2.1 MATLAB package	Danuser laboratory	http://lccb.hms.harvard.edu/software.html

RESOURCE AVAILABILITY

Lead contact

Further information and requests for resources and reagents should be directed to and will be fulfilled by the lead contract, Fabio Falleroni (fabio.falleroni@tum.de).

Materials availability

All requests for resources and reagents should be directed to and will be fulfilled by the lead contract, Fabio Falleroni (fabio.falleroni@tum.de).

Data and code availability

- All data reported in this paper will be shared by the lead contact upon request.
- This paper does not report original codes.
- Any additional information required to reanalyze the data reported in this paper is available from the lead contact upon request.

EXPERIMENTAL MODEL AND SUBJECT DETAILS

Hippocampal neuronal culture

Hippocampal neurons from post-natal day 2 (P2) Wistar rats were prepared in accordance with the guidelines of the Italian Animal Welfare Act, and their use was approved by the Local Veterinary Service, the

SISSA Ethics Committee board and the National Ministry of Health (Permit Number: 2848-III/15) in accordance with the European Union guidelines for animal care (d.l. 26, March 4th 2014 related to 2010/63/UE and d.1. 116/92; 86/609/C.E.). The sex of each rat was not verified. The animals were anesthetized with CO2 and sacrificed by decapitation, and all efforts were made to minimize suffering. Next, neurons were plated on coverslips coated with 50 μg/mL poly-L-ornithine (Sigma-Aldrich) and incubated (5% CO_2, 37°C) for 24-48 h in Neurobasal medium (Thermo Fisher) supplemented with 0.5 mM GlutaMAX and 2% B27 supplement (Thermo Fisher).

METHOD DETAILS

Calcium imaging experiment

Neurons were loaded with the cell-permeable calcium dye Fluo4-AM (Life Technologies, #F14201). Briefly, the cells were incubated with 20% Fluo4-AM and Pluronic F-127 in Krebs-Ringer's solution containing 119 mM NaCl, 2.5 mM KCl, 1 mM NaH_2PO_4, 2.5 mM $CaCl_2$, 1.3 mM $MgCl_2$, 11 mM D-glucose, 1.3 mM $MgCl_2$, and 20 mM HEPES (pH 7.4) at 37 °C for 30 min. After incubation, the cultures were washed two times and then transferred to the stage of an Olympus IX-81 inverted microscope. The experiments were performed at 37 °C, and images were acquired using Micromanager software with an Apo-Fluor 60x/1.2 NA objective at a sampling rate of 5 Hz (LED illumination (λ = 480 nm). Imaging experiments were conducted with Krebs-Ringer's solution (pH 7.4). We monitored possible evoked $[Ca^{2+}]_i$ changes by analysing F, and we focused on the evoked fractional change of fluorescence DF/F= $(F_{stim}-F_{unstim})/F_{unstim}$), where F_{stim} is the fluorescence following mechanical stimulation and F_{unstim} is the fluorescence averaged in a time period of 1 sec before mechanical stimulation (Figure 1B) in the ROI indicated by the light grey box (the second panel in Figure 1B).

Optical manipulation

To mechanically stimulate the cell, we used a custom-built optical tweezer combined with an inverted microscope (Olympus IX81). Briefly, we used a polystyrene bead with a 3.5 μm diameter (Sigma-Aldrich) optically trapped in a controllable oscillatory optical trap (OOT). We used an infrared (IR) laser at 1064 nm for trapping (IPG Laser Germany). The axial position of the trap could be adjusted within a range of 0–20 μm using a custom designed two-lens system composed of a focus tunable lens (FTL) (EL-10-30-NIR-LD, Optotune AG), of which the focal length can be varied by computer control (LabVIEW software).

Force and indentation measurement

The force exterted by the bead on the cell membrane can be measured by measured using the Back-Plane Interferometry (BFI) technique (Neuman and Block, 2004). In the BFI method, the interference of the laser light scattered by the bead in the optical trap allows for the bead to be used as a position probe and, through the assumption of a parabolic potential for the optical trap, a force probe. Thus, the displacement of the bead in the trap was followed from the displacement of the interference pattern on the QPD, which could be measured at frequencies of tens of kHz. When the displacement, is less than 500 nm, it can be related to the force, F exerted on the bead (which is equal to the force exerted by the bead on the cell) by a proportionality factor, k: $F = k \cdot S$ where the k is called elastic constant or trap stiffness.

Electrophysiology

Whole-cell currents were recorded using borosilicate glass pipette with a resistance of 2-5 MΩ filled with intracellular solution containing (in mM): 10 NaCl, 140 KCl, 1 $Mgcl_2$, 5 EGTA and 10 HEPES. Briefly, we used a manual micromanipulator to move vertically the patch clamp pipette in contact with the cell membrane about 5 μm from the mechanical stimulation site. After reaching a seal between the membrane and the electrode of more than 1 GΩ resistance, we applied a gentle suction to break the membrane patch in order to enter in whole-cell configuration. To confirm the integrity of the whole-cell configuration, we induced voltage gated Na^+ and K^+ currents by depolarizing the cell with voltage steps from −80 mV to +80 mV (10 mV increments). Then, we proceeded with the simultaneous cell mechanical stimulation with forces in the range of 10-50 pN and the characterization of the responses in the whole-cell configuration. For all experiments, the cells were bathed in an extracellular solution containing in mM 140 NaCl, 2.8 KCl, 1 $MgCl_2$, 2 $CaCl_2$ and 10 HEPES and maintained at a holding potential of −80 mV. The experiments were performed at 37 °C.

Immunofluorescence analysis

For the immunofluorescence analysis of Piezo1 and Piezo2, the cells were fixed with 4% paraformaldehyde for 10 min, permeabilized with 0.1% Triton X-100 (Merck, #X100) for 10 min, blocked with 1% BSA (Sigma-Aldrich #A7030) for 30 min. Primary antibodies against Piezo1 (Alomone Labs, #APC-087) and Piezo2 (Alomone Labs, #APC-090) were incubated in PBS for 3 h at room temperature. Goat anti-rabbit secondary antibody, P conjugate, was used at a concentration of μg/mL in phosphate buffered saline containing 0.2% BSA for 1 h at room temperature. Nuclei were stained with DAPI. The neuronal component was stained with Tuji-1 (Sigma-Aldrich, #T3952)). The images were captured at 40X magnification using Eclipse Series TiE, equipped with a C1 confocal.

FRET measurements

Hippocampal neurons were transfected 24 h after the dissection with the intramolecular CAMKII/RhoA FRET sensors using Lipofec-tamine 2000. Transfections were carried out according to manufacturer instructions using OptiMEM reduced-serum medium (Gibco, #51985034). The medium was refreshed 6 h after transfection. Then, cells were cultured for another 12–24 h before experiments were performed. For FRET ratiometric experiments, the following plasmids were used: pcDNA3- Camuiα -CR (Addgene plasmid, #40256) and pCAGGS-Raichu-RhoA-CR (Addgene plasmid, #40258). Time-lapse images were taken using an 60X oil immersion objective (Olympus, NA = 1.4). All acquisitions were done with a CCD dual sensor at 2 fps (ORCA–D2, Hamamatsu).

QUANTIFICATION AND STATISTICAL ANALYSIS

GraphPad Prism and Origin software were used for all statistical analysis. All central tendency values are mean and error bars shown are standard deviation of the mean. In all case, at least three independent experimental repeats were carried out for each condition. Calcium imaging experiments were processed with the ImageJ macros dFoverFmovie (https://gist.github.com/ackman678/5817461). Electrophysiological data were processed, analyzed, and baseline corrected with Clampfit 10.3 (Molecular Devices). For FRET experiments the ratiometric corrections and ratio calculations to generate cctivity images were performed using the Biosensor 2.1 MATLAB package (Danuser laboratory: http://lccb.hms.harvard.edu/software.html).

ADDITIONAL RESOURCES

This study has not generated or contributed to a new website/forum and is not part of a clinical trial.